*J. Fluid Mech.* (2000), *vol.* 407, *pp.* 1–26. Printed in the United Kingdom



# Analysis and modelling of turbulent flow in an axially rotating pipe

By C. G. SPEZIALE[1]†, B. A. YOUNIS[2] AND S. A. BERGER[3]

[1]Aerospace and Mechanical Engineering Department, Boston University, Boston, MA 02215, USA
[2]Department of Civil Engineering, City University, London ECIV 0HB, UK
[3]Department of Mechanical Engineering, University of California, Berkeley, Berkeley, CA 94720, USA

(Received 1 December 1997 and in revised form 2 October 1999)

The analysis and modelling of the structure of turbulent flow in a circular pipe subjected to an axial rotation is presented. Particular attention is paid to determining the terms in various turbulence closures that generate the two main physical features that characterize this flow: a rotationally dependent axial mean velocity and a rotationally dependent mean azimuthal or swirl velocity relative to the rotating pipe. It is shown that the first feature is well represented by two-dimensional explicit algebraic stress models but is irreproducible by traditional two-equation models. On the other hand, three-dimensional frame-dependent models are needed to predict the presence of a mean swirl velocity. The latter is argued to be a secondary effect which arises from a cubic nonlinearity in standard algebraic models with conventional near-wall treatments. Second-order closures are shown to give a more complete description of this flow and can describe both of these features fairly well. In this regard, quadratic pressure–strain models perform the best overall when extensive comparisons are made with the results of physical and numerical experiments. The physical significance of this problem and the implications for future research in turbulence are discussed in detail.

## 1. Introduction

Turbulent flow in pipes has been a popular benchmark case for the testing and evaluation of both theories and models of turbulence during the past century. One of the first notable examples was the mixing length theory of Prandtl (1925) which was partially validated using early turbulent pipe flow data approximately seventy years ago. Laufer (1954) probably provided the first extensive measurements of the fully developed turbulence structure in a stationary circular pipe. Then an interest arose in laminar pipe flow subjected to a spanwise rotation with its associated secondary flows (Benton 1956). This was of geophysical interest since the Earth's rotation gives rise to a spanwise rotation. The turbulent version of this problem later received considerable attention also (Majumder, Pratap & Spalding 1977; Howard, Patankar & Bordynuik 1980). This problem is primarily characterized by the development of a double-vortex secondary flow in planes perpendicular to the axial velocity in the frame of the rotating pipe. It also has an analogy with flow in a curved pipe (Dennis

† Professor Speziale died in April 1999 while this paper was being revised.

& Ng 1982; Berger, Talbot & Yao 1983). More recently, the problem of turbulent flow in an axially rotating pipe has come to be of considerable interest. The laminar counterpart of this problem is not of interest since – relative to the rotating pipe – the flow is unidirectional with a parabolic velocity profile. Thus, the laminar flow problem with an axial rotation is identical to its non-rotating counterpart. However, for fully developed turbulent flow there is a decided difference. Relative to an observer who is rotating with the pipe, the flow is no longer unidirectional in the mean or averaged sense. There is a non–zero azimuthal component of the mean velocity that is present. Thus, there is a secondary flow in the form of a mean swirl velocity. The continuity equation forces the radial mean velocity to be zero, under fully developed conditions with azimuthal symmetry, so there is just one other component of the mean velocity in addition to the axial component. Furthermore, both these components are rotationally dependent, varying significantly with the rotation rate of the pipe.

The literature contains a number of well-documented experiments which include the measurements of Murakami & Kikuyama (1980), Kikuyama, Murakama & Nishibori (1983*a*), Reich & Beer (1989) and, most recently, those of Imao, Itoh & Harada (1996). Calculations of this flow, with the use of a variety of turbulence closures, have been reported by Kikuyama *et al.* (1983*b*), Hirai, Takagi & Matsumato (1988) and Malin & Younis (1997). More recently, direct and large-eddy simulations were conducted of turbulent flow in an axially rotating pipe, for example by Eggels, Boersma & Nieuwstadt (1994, see also Eggels & Nieuwstadt 1993) which further illuminated this flow. In the last year, Orlandi & Fatica (1997) have conducted extensive, well-resolved direct simulations that are an excellent addition to the published work on this flow. This problem is of considerable practical importance because of the analogies with three-dimensional turbulent boundary layers such as those on the swept wings of aircraft. It is, furthermore, of value in the understanding of swirling flows which have important applications in combustion as well as in other fields.

In this paper, the analysis and modelling of turbulent flow in an axially rotating pipe will be presented in detail. The focus will be on the systematic analysis of the key features of various turbulence models that determine their performance in this flow. The generators for the principal effects in an axially rotating pipe will be clearly identified. This flow is rapidly becoming an important benchmark problem for the verification of turbulence models and hence the present motivation in identifying the underlying physical processes and examining their consequences for modelling strategies. It will be shown that traditional two-equation models are fundamentally incapable of describing this flow as far as its main physical attributes are concerned. The two most important physical features are a rotationally dependent axial velocity and the presence of a rotationally dependent azimuthal or swirl velocity in the mean relative to the rotating pipe. Traditional two-equation models – such as the standard $K$–$\varepsilon$ model – fail to predict both effects. The first effect (the rotationally dependent axial mean velocity) will be shown to be well described by two-dimensional explicit algebraic stress models which only have a quadratic tensorial nonlinearity. While such models, with conventional near-wall treatments, are incapable of describing the presence of a mean swirl velocity (the second feature mentioned), it is argued that this is not an extremely serious drawback in that such a mean swirl velocity only constitutes an effect that is approximately 15% of the axial mean velocity. It is decisively shown that to predict the presence of a mean swirl velocity for this flow problem with standard algebraic models, a cubic nonlinearity is needed as has been argued previously (Wallin & Johansson 1997, see also Wallin & Johansson 2000). On the other hand, second-order closures can predict both effects with a linear

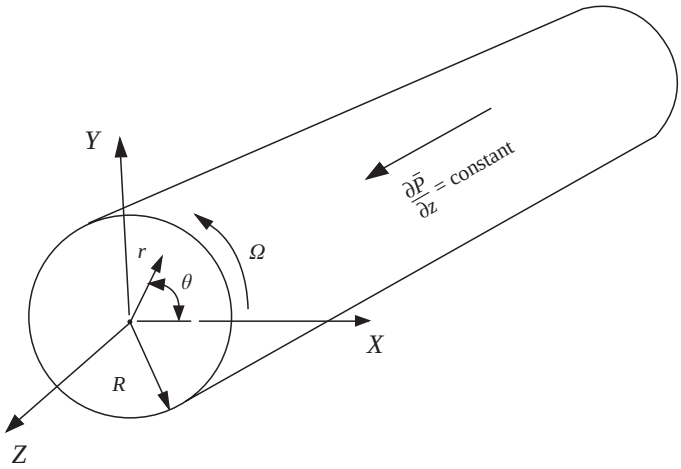


FIGURE 1. Schematic of turbulent flow in an axially rotating circular pipe.

pressure–strain model (which in the three-dimensional equilibrium limit gives rise to an algebraic model with a quartic nonlinearity through the algebraic stress model approximation). However, it will be shown – by making extensive comparisons with the results of physical and numerical experiments – that quadratic pressure–strain models perform the best overall. In this regard, calculations with the Launder, Reece & Rodi (1975) and Speziale, Sarkar & Gatski (1991) models will be presented. Pettersson, Andersson & Brunvoll (1998) recently demonstrated that cubic pressure–strain models, despite their complexity, do not perform as well in this problem. Interestingly enough, Younis, Gatski & Speziale (1996) showed that another problem with swirl – the swirling free jet – is also better described with a quadratic pressure–strain model.

Particular attention will be paid to tracing the origins of each of the two central physical features in an axially rotating pipe in order to gain a better physical insight into this turbulent flow. Furthermore, detailed model calculations will be presented and it will be demonstrated that the presence of a mean swirl velocity is a near-wall effect at high Reynolds numbers (at high Reynolds numbers, in the absence of solid boundaries, the solution is the same as the inviscid case). Owing to the analogies that are sometimes made between the laminar flow of a non-Newtonian fluid and the mean turbulent flow of a Newtonian fluid, the laminar non-Newtonian version of this problem was also considered, along with the associated questions of invariance which have considerable relevance to this problem. As stated earlier, this flow is of significant technological relevance and is one that is becoming an important benchmark case. This provides the motivation for its study from a theoretical standpoint, something that has not been done before. The current status of modelling, and the prospects for future research in turbulence will be thoroughly discussed in the sections to follow.

## 2. Theoretical background

To analyse flow in an axially rotating circular pipe of radius $R$, we consider the Navier–Stokes and continuity equations in a steadily rotating frame – about the axial direction – written in cylindrical coordinates (see the schematic diagram shown in figure 1). For the three-dimensional velocity field $\boldsymbol{u} = u_r(r, \theta, z, t)\boldsymbol{e}_r + u_\theta(r, \theta, z, t)\boldsymbol{e}_\theta +$

$u_z(r,\theta,z,t)\boldsymbol{e}_z$, they take the form (Batchelor 1967)

$$\frac{\partial u_r}{\partial t}+\boldsymbol{u}\cdot\nabla u_r-\frac{u_\theta^2}{r}=-\frac{\partial P}{\partial r}+\nu\left(\nabla^2 u_r-\frac{u_r}{r^2}-\frac{2}{r^2}\frac{\partial u_\theta}{\partial\theta}\right)+2\Omega u_\theta, \tag{1}$$

$$\frac{\partial u_\theta}{\partial t}+\boldsymbol{u}\cdot\nabla u_\theta+\frac{u_r u_\theta}{r}=-\frac{1}{r}\frac{\partial P}{\partial\theta}+\nu\left(\nabla^2 u_\theta-\frac{u_\theta}{r^2}+\frac{2}{r^2}\frac{\partial u_r}{\partial\theta}\right)-2\Omega u_r, \tag{2}$$

$$\frac{\partial u_z}{\partial t}+\boldsymbol{u}\cdot\nabla u_z=-\frac{\partial P}{\partial z}+\nu\nabla^2 u_z, \tag{3}$$

$$\frac{1}{r}\frac{\partial(ru_r)}{\partial r}+\frac{1}{r}\frac{\partial u_\theta}{\partial\theta}+\frac{\partial u_z}{\partial z}=0. \tag{4}$$

In (1)–(3), $P$ is the modified pressure that contains the centrifugal and gravitational body force potentials, $\nu$ is the kinematic viscosity, and $\boldsymbol{\Omega}\equiv\Omega\boldsymbol{e}_z$ is the rotation rate of the frame which is undergoing an axial rotation with the pipe so that there are Coriolis effects. These equations are solved subject to the no-slip condition $\boldsymbol{u}(R,\theta,z,t)=0$ on the walls of the pipe. As will be seen later, the analysis of this flow is substantially simplified by the choice of a coordinate system that rotates with the pipe.

In order to obtain the instantaneous turbulent fields, (1)–(4) must be solved numerically since the turbulence is three-dimensional and time-dependent. The laminar flow version of this problem has a fully developed unidirectional solution in the form of a parabolic velocity profile (Batchelor 1967)

$$u_z=\frac{G}{4\nu}(R^2-r^2), \tag{5}$$

where $-G$ is the constant axial pressure gradient that drives the flow. Thus, this solution is identical to that in a stationary pipe, as mentioned earlier, which is why the laminar version of this problem is not of interest. The laminar solution (5) has been found to be stable provided that the Reynolds number is sufficiently small. No bifurcation or symmetry breaking bifurcation in the solution has been found at low Reynolds numbers in the laminar regime.

Since we are interested in the turbulence modelling aspects of this problem, we will consider the Reynolds-averaged form of the Navier–Stokes and continuity equations which here take the form (Hinze 1975)

$$\begin{aligned}\bar{\boldsymbol{u}}\cdot\nabla\bar{u}_r-\frac{\bar{u}_\theta^2}{r}=&-\frac{\partial\overline{P}}{\partial r}+\nu\left(\nabla^2\bar{u}_r-\frac{\bar{u}_r}{r^2}-\frac{2}{r^2}\frac{\partial\bar{u}_\theta}{\partial\theta}\right)\\&-\frac{\partial\tau_{rr}}{\partial r}-\frac{1}{r}\frac{\partial\tau_{r\theta}}{\partial\theta}-\frac{\partial\tau_{rz}}{\partial z}-\frac{1}{r}(\tau_{rr}-\tau_{\theta\theta})+2\Omega\bar{u}_\theta,\end{aligned} \tag{6}$$

$$\begin{aligned}\bar{\boldsymbol{u}}\cdot\nabla\bar{u}_\theta+\frac{\bar{u}_r\bar{u}_\theta}{r}=&-\frac{1}{r}\frac{\partial\overline{P}}{\partial\theta}+\nu\left(\nabla^2\bar{u}_\theta-\frac{\bar{u}_\theta}{r^2}+\frac{2}{r^2}\frac{\partial\bar{u}_r}{\partial\theta}\right)\\&-\frac{\partial\tau_{r\theta}}{\partial r}-\frac{1}{r}\frac{\partial\tau_{\theta\theta}}{\partial\theta}-\frac{\partial\tau_{\theta z}}{\partial z}-\frac{2}{r}\tau_{r\theta}-2\Omega\bar{u}_r,\end{aligned} \tag{7}$$

$$\bar{\boldsymbol{u}}\cdot\nabla\bar{u}_z=-\frac{\partial\overline{P}}{\partial z}+\nu\nabla^2\bar{u}_z-\frac{\partial\tau_{rz}}{\partial r}-\frac{1}{r}\frac{\partial\tau_{\theta z}}{\partial\theta}-\frac{\partial\tau_{zz}}{\partial z}-\frac{1}{r}\tau_{rz}, \tag{8}$$

$$\frac{1}{r}\frac{\partial(r\bar{u}_r)}{\partial r}+\frac{1}{r}\frac{\partial\bar{u}_\theta}{\partial\theta}+\frac{\partial\bar{u}_z}{\partial z}=0, \tag{9}$$

where an overbar represents a Reynolds-averaged quantity, and $\tau_{ij} = \overline{u'_i u'_j}$ is the Reynolds stress tensor.

While the general problem of a flow in an axially rotating pipe is fully three-dimensional (in the sense that all three velocity components are finite), we confine consideration here to the fully developed flow with azimuthal symmetry where the flow substantially simplifies. Since the geometry and boundary conditions exhibit azimuthal symmetry, one would expect the mean flow to do the same unless there is a symmetry-breaking bifurcation, which has not been observed either experimentally or computationally. Hence, under fully developed conditions we expect there to be a mean flow solution of the form $\bar{\boldsymbol{u}} = \bar{\boldsymbol{u}}(r)$. Then the mean continuity equation (9) reduces to

$$\frac{1}{r}\frac{\mathrm{d}(r\bar{u}_r)}{\mathrm{d}r} = 0, \tag{10}$$

which has the solution

$$\bar{u}_r = \frac{C_1}{r} \tag{11}$$

where $C_1$ is a constant. The no-slip boundary condition $\bar{\boldsymbol{u}}(R) = 0$ – along with the condition of regularity of the velocity field at $r = 0$ – yields $C_1 = 0$ and, hence, $\bar{u}_r = 0$. Thus, $\bar{\boldsymbol{u}} = \bar{u}_\theta(r)\boldsymbol{e}_\theta + \bar{u}_z(r)\boldsymbol{e}_z$ and the mean continuity equation (9) is satisfied *identically* for a fully developed mean turbulent flow that is azimuthally symmetric. The Reynolds-averaged Navier–Stokes equations then become, since $\bar{u}_r = 0$ and $\bar{\boldsymbol{u}} \cdot \nabla = 0$,

$$-\frac{\bar{u}_\theta^2}{r} = -\frac{\partial \overline{P}}{\partial r} - \frac{\mathrm{d}\tau_{rr}}{\mathrm{d}r} - \frac{1}{r}(\tau_{rr} - \tau_{\theta\theta}) + 2\Omega\bar{u}_\theta, \tag{12}$$

$$\nu\left(\nabla^2\bar{u}_\theta - \frac{\bar{u}_\theta}{r^2}\right) - \frac{\mathrm{d}\tau_{r\theta}}{\mathrm{d}r} - \frac{2}{r}\tau_{r\theta} = 0, \tag{13}$$

$$-\frac{\partial \overline{P}}{\partial z} + \nu\nabla^2\bar{u}_z - \frac{\mathrm{d}\tau_{rz}}{\mathrm{d}r} - \frac{1}{r}\tau_{rz} = 0, \tag{14}$$

where the Laplacian simplifies to

$$\nabla^2 = \frac{1}{r}\frac{\mathrm{d}}{\mathrm{d}r}\left(r\frac{\mathrm{d}}{\mathrm{d}r}\right).$$

Equation (12) simply sets the radial dependence of the pressure that is needed to maintain the flow (note that $\overline{P} = \overline{P}(r, z)$; $\partial\overline{P}/\partial z$ is a constant). The mean axial and swirl velocities are obtained from (13) and (14).

From (13) it is clear that a non-zero mean swirl velocity is generated by the shear component $\tau_{r\theta}$ of the Reynolds stress tensor which is a source term in this equation. In order to guarantee that this component is non-zero and that the flow is not unidirectional – as indicated by experiments – a non-zero $\tau_{r\theta}$ Reynolds shear stress must be generated by the axial mean velocity $\bar{u}_z(r)$. *In more precise terms, a mean swirl velocity $\bar{u}_\theta(r)$ is generated in a fully-developed axially rotating pipe flow when the axial mean velocity $\bar{u}_z = \bar{u}_z(r)$ gives rise to a non-zero Reynolds shear stress $\tau_{r\theta}$, independently of the swirl velocity*. This proposition is at variance with the commonly held belief (e.g. Hirai *et al.* 1988) that adoption of a gradient-type assumption for the turbulent transport of tangential momentum is responsible for the failure of the standard $K$–$\varepsilon$ model to generate a non-zero swirl velocity. Hirai *et al.* arrived at this conclusion by setting the viscous term in (13) to zero. This is an inappropriate approximation in a flow such as this one where the viscous term makes an important contribution in the

near-wall region. *We further propose that the mean swirl velocity – as well as the axial mean velocity – will be rotationally dependent if both Reynolds shear stress components* $\tau_{r\theta}$ *and* $\tau_{rz}$ *depend on the rotation rate* $\Omega$ *of the pipe.* It is clear from (14) that $\tau_{rz}$ serves as a source term for the axial mean velocity. Such a rotational dependence is expected from the Reynolds stress transport equation although it is often missing in simpler models such as the standard $K$–$\varepsilon$ model of turbulence.

Initially we had thought that further light could be shed on this flow by examination of the analogous problem of laminar, non-Newtonian flow in an axially-rotating pipe. However, it turns out that a simple non-Newtonian analogy does not provide an adequate description of this flow (see the Appendix). Adoption of a frame-dependent model would therefore appear to be essential for the main features of this flow to be correctly predicted. One has frame-dependent models whenever there is not a clear-cut separation of scales such as in turbulent flows (Speziale 1998*b*). The primary reason that the standard $K$–$\varepsilon$ model does not provide a good description of this flow is that it is frame-indifferent, as will be discussed in the next section.

## 3. Generators for swirl and a rotationally dependent mean velocity in the axially rotating pipe

In this section, it will be shown what terms generate a non-zero mean swirl velocity and a rotationally dependent axial mean velocity in axially rotating turbulent pipe flow – the two main physical effects in this problem. Use will be made of the results of the last section where it was shown that a swirl velocity is generated when the axial mean velocity gives rise to a non-zero Reynolds shear stress $\tau_{r\theta}$. The axial mean velocity – along with the mean swirl velocity – will be rotationally dependent if both $\tau_{r\theta}$ and $\tau_{rz}$ depend on the rotation rate $\Omega$ of the pipe. Both two-equation models and full second-order closures will be considered.

### 3.1. *Traditional two-equation models*

The standard and nonlinear $K$–$\varepsilon$ models will be considered in detail. The standard $K$–$\varepsilon$ model consists of the eddy viscosity representation for the Reynolds stress tensor which, in coordinate–free notation, reads

$$\boldsymbol{\tau} = \tfrac{2}{3}K\boldsymbol{I} - 2\nu_T\overline{\boldsymbol{S}}. \tag{15}$$

where $\boldsymbol{I}$ is the unit tensor and $\overline{\boldsymbol{S}}$ is the mean strain rate tensor.

The turbulent kinetic energy $K$ and turbulent dissipation rate $\varepsilon$ are obtained from separate modelled transport equations. These equations take the general form

$$\frac{\partial K}{\partial t} + \bar{\boldsymbol{u}}\cdot\nabla K = \mathscr{P} - \varepsilon + \frac{\partial}{\partial x_i}\left(\frac{\nu_T}{\sigma_k}\frac{\partial K}{\partial x_i}\right), \tag{16}$$

$$\frac{\partial \varepsilon}{\partial t} + \bar{\boldsymbol{u}}\cdot\nabla \varepsilon = C_{\varepsilon 1}\frac{\varepsilon}{K}\mathscr{P} - C_{\varepsilon 2}\frac{\varepsilon^2}{K} + \frac{\partial}{\partial x_i}\left(\frac{\nu_T}{\sigma_\varepsilon}\frac{\partial \varepsilon}{\partial x_i}\right), \tag{17}$$

where $\mathscr{P} \equiv -\tau_{ij}\partial\bar{u}_i/\partial x_j$ is the turbulence production and $C_{\varepsilon 1}$, $C_{\varepsilon 2}$, $\sigma_k$ and $\sigma_\varepsilon$ are constants. The standard $K$–$\varepsilon$ model is frame-indifferent, i.e. it takes the same form in all frames of reference independently of whether or not they are inertial (Speziale 1998*b*). We will write the Reynolds stress tensor – as well as other tensors – in matrix

form making use of cylindrical coordinates. Thus, for example,

$$\boldsymbol{\tau} = \begin{pmatrix} \tau_{rr} & \tau_{r\theta} & \tau_{rz} \\ \tau_{r\theta} & \tau_{\theta\theta} & \tau_{\theta z} \\ \tau_{rz} & \tau_{\theta z} & \tau_{zz} \end{pmatrix}. \tag{18}$$

In cylindrical coordinates, the mean rate-of-strain tensor that the axial mean velocity gives rise to takes the form

$$\overline{\boldsymbol{S}} = \begin{pmatrix} 0 & 0 & \frac{1}{2}\mathrm{d}\bar{u}_z/\mathrm{d}r \\ 0 & 0 & 0 \\ \frac{1}{2}\mathrm{d}\bar{u}_z/\mathrm{d}r & 0 & 0 \end{pmatrix}. \tag{19}$$

It is clear, therefore, that $\tau_{r\theta} = -2\nu_T \overline{S}_{r\theta} = 0$ and the axial mean velocity does not generate a non-zero Reynolds shear stress. *Thus, the standard $K$–$\varepsilon$ model does not yield a non-zero mean swirl velocity by virtue of* (*13*), (*19*) *and, as such, is inconsistent with physical and numerical experiments.* Furthermore, since it is frame-indifferent, the standard $K$–$\varepsilon$ model does not yield the rotationally dependent axial mean velocity shown by experiments. These deficiencies will be demonstrated by calculations later. It is worth noting that these deficiencies are shared by all eddy viscosity models based on the Boussinesq hypothesis.

The nonlinear $K$–$\varepsilon$ model of Speziale (1987) takes the form

$$\tau_{ij} = \tfrac{2}{3}K\delta_{ij} - 2C_\mu \frac{K^2}{\varepsilon}\overline{S}_{ij} - 4C_D C_\mu^2 \frac{K^3}{\varepsilon^2}\left(\overline{S}_{ik}\overline{S}_{kj} - \tfrac{1}{3}\overline{S}_{mn}\overline{S}_{mn}\delta_{ij}\right) - 4C_E C_\mu^2 \frac{K^3}{\varepsilon^2}\left(\overset{\circ}{\overline{S}}_{ij} - \tfrac{1}{3}\overset{\circ}{\overline{S}}_{mm}\,\delta_{ij}\right), \tag{20}$$

where, for steady flows,

$$\overset{\circ}{\overline{S}}_{ij} = \bar{u}_k \frac{\partial \overline{S}_{ij}}{\partial x_k} - \frac{\partial \bar{u}_i}{\partial x_k}\overline{S}_{kj} - \frac{\partial \bar{u}_j}{\partial x_k}\overline{S}_{ki} \tag{21}$$

is the frame-indifferent Oldroyd derivative of $\overline{S}_{ij}$ and $C_D$ and $C_E$ are constants (Speziale 1987). In coordinate–free notation

$$\boldsymbol{\tau} = \tfrac{2}{3}K\boldsymbol{I} - 2C_\mu \frac{K^2}{\varepsilon}\overline{\boldsymbol{S}} - 4C_D C_\mu^2 \frac{K^3}{\varepsilon^2}\left[\overline{\boldsymbol{S}}^2 - \tfrac{1}{3}\mathrm{tr}\,(\overline{\boldsymbol{S}}^2)\boldsymbol{I}\right] - 4C_E C_\mu^2 \frac{K^3}{\varepsilon^2}\left[\overset{\circ}{\overline{\boldsymbol{S}}} - \tfrac{1}{3}\mathrm{tr}\,(\overset{\circ}{\overline{\boldsymbol{S}}})\boldsymbol{I}\right], \tag{22}$$

where $\mathrm{tr}\,(\cdot)$ denotes the trace. It is a simple matter to show that the axial mean velocity yields

$$\overline{\boldsymbol{S}}^2 = \begin{pmatrix} \frac{1}{4}\left(\mathrm{d}\bar{u}_z/\mathrm{d}r\right)^2 & 0 & 0 \\ 0 & 0 & 0 \\ 0 & 0 & \frac{1}{4}\left(\mathrm{d}\bar{u}_z/\mathrm{d}r\right)^2 \end{pmatrix} \tag{23}$$

and

$$\nabla\bar{\boldsymbol{u}} = \begin{pmatrix} 0 & 0 & \mathrm{d}\bar{u}_z/\mathrm{d}r \\ 0 & 0 & 0 \\ 0 & 0 & 0 \end{pmatrix}. \tag{24}$$

From (21), the axial mean velocity gives rise to

$$\overset{\circ}{\overline{\boldsymbol{S}}} = \begin{pmatrix} 0 & 0 & 0 \\ 0 & 0 & 0 \\ 0 & 0 & -\left(\mathrm{d}\bar{u}_z/\mathrm{d}r\right)^2 \end{pmatrix}. \tag{25}$$

It is thus clear from (19), (22), (23) and (25) that $\tau_{r\theta} = 0$ and the nonlinear $K$–$\varepsilon$ model does not generate a non-zero mean swirl velocity. Furthermore, since it is frame-indifferent (Speziale 1998*b*), the nonlinear $K$–$\varepsilon$ model does not predict a rotationally dependent axial mean velocity, since $\tau_{rz}$ is independent of $\Omega$, in contradiction to experiments. *Thus, the standard and nonlinear $K$–$\varepsilon$ models – like all traditional two-equation models with conventional near-wall treatments – are incapable of predicting the main physical features of turbulent flow in an axially rotating pipe.* The nonlinear $K$–$\varepsilon$ model was developed relative to material frame–indifference in the limit of two-dimensional turbulence. Since it is an algebraic model, the model exactly satisfies material frame–indifference in the limit of two-dimensional turbulence. That is why the Oldroyd derivative is present. This constraint is far too severe in the context of practical closure models and hence an alternative form such as the explicit algebraic stress model (presented below) is a far better alternative, even though it collapses to the nonlinear $K$–$\varepsilon$ model for certain basic flows in an inertial frame (Gatski & Speziale 1993). Frame-dependent terms are needed to describe the axially rotating pipe. In the next section illustrative calculations will be provided that demonstrate these points.

### 3.2. *Explicit algebraic stress models*

In this subsection we present an analysis of explicit algebraic stress models obtained from the Reynolds stress transport equation by solving the implicit algebraic equations that result from the algebraic stress model approximation for equilibrium turbulent flows (Gatski & Speziale 1993). They are in the resultant form of anisotropic eddy viscosity models with strain-dependent coefficients. The specific form of the explicit algebraic stress models, for two-dimensional mean turbulent flows, is

$$\tau_{ij} = \tfrac{2}{3}K\delta_{ij} - \frac{3}{3-2\eta^2+6\xi^2}\left[\alpha_1\frac{K^2}{\varepsilon}\overline{S}_{ij} + \alpha_2\frac{K^3}{\varepsilon^2}(\overline{S}_{ik}\overline{W}_{kj} + \overline{S}_{jk}\overline{W}_{ki}) - \alpha_3\frac{K^3}{\varepsilon^2}\left(\overline{S}_{ik}\overline{S}_{kj} - \tfrac{1}{3}\overline{S}_{k\ell}\overline{S}_{k\ell}\delta_{ij}\right)\right], \tag{26}$$

where $\alpha_1, \alpha_2$ and $\alpha_3$ are constants. More specifically,

$$\left.\begin{aligned} &\alpha_1 = (\tfrac{4}{3} - C_2)g, \quad \alpha_2 = \tfrac{1}{2}(\tfrac{4}{3} - C_2)(2 - C_4)g^2, \quad \alpha_3 = (\tfrac{4}{3} - C_2)(2 - C_3)g^2, \\ &g = \left(\tfrac{1}{2}C_1 + \frac{\mathscr{P}}{\varepsilon} - 1\right)^{-1}, \quad \eta = \frac{1}{2}\frac{\alpha_3}{\alpha_1}\frac{K}{\varepsilon}(\overline{S}_{ij}\overline{S}_{ij})^{1/2}, \quad \xi = \frac{\alpha_2}{\alpha_1}\frac{K}{\varepsilon}(\overline{W}_{ij}\overline{W}_{ij})^{1/2}, \end{aligned}\right\} \tag{27}$$

and $\mathscr{P}/\varepsilon$ is usually specified to be 1 in wall-bounded turbulent flows. Here,

$$\overline{W}_{ij} = \frac{1}{2}\left(\frac{\partial\bar{u}_i}{\partial x_j} - \frac{\partial\bar{u}_j}{\partial x_i}\right) + \left(\frac{C_4 - 4}{C_4 - 2}\right)e_{mji}\Omega_m, \tag{28}$$

where $e_{ijk}$ is the permutation tensor and $C_1$–$C_4$ are constants in the pressure–strain model that will be discussed later. For the SSG model, the coefficients $C_1$–$C_4$ take on the respective equilibrium values of 4.80, 0.36, 1.25 and 0.40. Explicit algebraic stress models are formally two-equation models since they are solved with modelled transport equations for $K$ and $\varepsilon$ that are of the same form as (16) and (17).

Since the strain-dependent expression in (26) is formally derived for turbulent flows that are in equilibrium, a singularity can arise in this coefficient in non-equilibrium turbulent flows through the vanishing of its denominator. Gatski & Speziale (1993)

proposed the simple regularization

$$\frac{3}{3-2\eta^2+\xi^2} \approx \frac{3(1+\eta^2)}{3+\eta^2+6\xi^2\eta^2+6\xi^2} \tag{29}$$

based on a Taylor expansion (more recently, Speziale & Xu 1996 considered regularized expressions via a Padé approximation that have some limited consistency with rapid distortion theory). This expression is approximately equivalent to the original expression for turbulent flows close to equilibrium – where it formally applies – and is regular and computable for all values of $\eta$ and $\xi$. With this regularization, the explicit algebraic stress model (26) takes the coordinate–free form

$$\boldsymbol{\tau} = \tfrac{2}{3}K\boldsymbol{I} - \frac{3(1+\eta^2)}{3+\eta^2+6\xi^2\eta^2+6\xi^2}\left[\alpha_1\frac{K^2}{\varepsilon}\overline{\boldsymbol{S}} + \alpha_2\frac{K^3}{\varepsilon^2}(\overline{\boldsymbol{S}}\,\overline{\boldsymbol{W}} - \overline{\boldsymbol{W}}\,\overline{\boldsymbol{S}})\right.$$
$$\left. -\alpha_3\frac{K^3}{\varepsilon^2}\left(\overline{\boldsymbol{S}}^2 - \tfrac{1}{3}\mathrm{tr}\,(\overline{\boldsymbol{S}}^2)\boldsymbol{I}\right)\right]. \tag{30}$$

The axial mean velocity gives rise to the following values of $\overline{\boldsymbol{W}}$:

$$\overline{\boldsymbol{W}} = \begin{pmatrix} 0 & -\alpha\Omega & -\frac{1}{2}\mathrm{d}\bar{u}_z/\mathrm{d}r \\ \alpha\Omega & 0 & 0 \\ \frac{1}{2}\mathrm{d}\bar{u}_z/\mathrm{d}r & 0 & 0 \end{pmatrix}, \tag{31}$$

where $\alpha \equiv (C_4-4)/(C_4-2)$. Therefore, the axial mean velocity yields the result

$$\overline{\boldsymbol{S}}\,\overline{\boldsymbol{W}} - \overline{\boldsymbol{W}}\,\overline{\boldsymbol{S}} = \begin{pmatrix} \frac{1}{2}\left(\mathrm{d}\bar{u}_z/\mathrm{d}r\right)^2 & 0 & 0 \\ 0 & 0 & -\frac{1}{2}\alpha\Omega\mathrm{d}\bar{u}_z/\mathrm{d}r \\ 0 & -\frac{1}{2}\alpha\Omega\mathrm{d}\bar{u}_z/\mathrm{d}r & -\frac{1}{2}\left(\mathrm{d}\bar{u}_z/\mathrm{d}r\right)^2 \end{pmatrix}. \tag{32}$$

An examination of (19), (23), (32) – in the light of (30) – establishes that $\tau_{r\theta} = 0$. Hence, since the two-dimensional explicit algebraic stress model does not generate a non-zero Reynolds shear stress $\tau_{r\theta}$ there will be no mean swirl velocity. However, unlike the standard and nonlinear $K$–$\varepsilon$ models, it does predict a rotationally dependent axial mean velocity, which is the more significant effect. Since

$$\tau_{rz} = -\frac{3\alpha_1(1+\eta^2)}{2(3+\eta^2+6\xi^2\eta^2+6\xi^2)}\frac{K^2}{\varepsilon}\frac{\mathrm{d}\bar{u}_z}{\mathrm{d}r}, \tag{33}$$

where

$$\eta = \frac{1}{2\sqrt{2}}\frac{\alpha_3}{\alpha_1}\frac{K}{\varepsilon}\frac{\mathrm{d}\bar{u}_z}{\mathrm{d}r}, \quad \xi = \frac{\alpha_2}{\alpha_1}\frac{K}{\varepsilon}\left[\frac{1}{2}\left(\frac{\mathrm{d}\bar{u}_z}{\mathrm{d}r}\right)^2 + 2\alpha^2\Omega^2\right]^{1/2},$$

it is clear that $\tau_{rz}$ – and, hence the axial mean velocity by virtue of (14) – will be rotationally dependent since it depends explicitly on $\Omega$ through $\xi$. In the next section, we will show illustrative calculations of this effect.

Although the explicit algebraic stress model (26) is formally derived for two-dimensional mean turbulent flows, it is often applied to three-dimensional flows (like the rotating axial pipe), sometimes with good results. The three-dimensional form of the explicit algebraic stress models is much more complicated. It takes the coordinate–free form (Pope 1975)

$$\boldsymbol{b}^* = \sum_{\lambda=1}^{10} G^{(\lambda)}\boldsymbol{T}^{(\lambda)} \tag{34}$$

where $\boldsymbol{T}^{(\lambda)}$ are the integrity bases given by

$$\left.\begin{array}{ll}
\boldsymbol{T}^{(1)} = \overline{\boldsymbol{S}}^{*}, & \boldsymbol{T}^{(6)} = \overline{\boldsymbol{W}}^{*2}\overline{\boldsymbol{S}}^{*} + \overline{\boldsymbol{S}}^{*}\overline{\boldsymbol{W}}^{*2} - \tfrac{2}{3}\{\overline{\boldsymbol{S}}^{*}\overline{\boldsymbol{W}}^{*2}\}\boldsymbol{I}, \\
\boldsymbol{T}^{(2)} = \overline{\boldsymbol{S}}^{*}\overline{\boldsymbol{W}}^{*} - \overline{\boldsymbol{W}}^{*}\overline{\boldsymbol{S}}^{*}, & \boldsymbol{T}^{(7)} = \overline{\boldsymbol{W}}^{*}\overline{\boldsymbol{S}}^{*}\overline{\boldsymbol{W}}^{*2} - \overline{\boldsymbol{W}}^{*2}\overline{\boldsymbol{S}}^{*}\overline{\boldsymbol{W}}^{*}, \\
\boldsymbol{T}^{(3)} = \overline{\boldsymbol{S}}^{*2} - \tfrac{1}{3}\{\overline{\boldsymbol{S}}^{*2}\}\boldsymbol{I}, & \boldsymbol{T}^{(8)} = \overline{\boldsymbol{S}}^{*}\overline{\boldsymbol{W}}^{*}\overline{\boldsymbol{S}}^{*2} - \overline{\boldsymbol{S}}^{*2}\overline{\boldsymbol{W}}^{*}\overline{\boldsymbol{S}}^{*}, \\
\boldsymbol{T}^{(4)} = \overline{\boldsymbol{W}}^{*2} - \tfrac{1}{3}\{\overline{\boldsymbol{W}}^{*2}\}\boldsymbol{I}, & \boldsymbol{T}^{(9)} = \overline{\boldsymbol{W}}^{*2}\overline{\boldsymbol{S}}^{*2} + \overline{\boldsymbol{S}}^{*2}\overline{\boldsymbol{W}}^{*2} - \tfrac{2}{3}\{\overline{\boldsymbol{S}}^{*2}\overline{\boldsymbol{W}}^{*2}\}\boldsymbol{I}, \\
\boldsymbol{T}^{(5)} = \overline{\boldsymbol{W}}^{*}\overline{\boldsymbol{S}}^{*2} - \overline{\boldsymbol{S}}^{*2}\overline{\boldsymbol{W}}^{*}, & \boldsymbol{T}^{(10)} = \overline{\boldsymbol{W}}^{*}\overline{\boldsymbol{S}}^{*2}\overline{\boldsymbol{W}}^{*2} - \overline{\boldsymbol{W}}^{*2}\overline{\boldsymbol{S}}^{*2}\overline{\boldsymbol{W}}^{*},
\end{array}\right\} \tag{35}$$

where $\{\cdot\}$ denotes the trace. Here,

$$b^{*}_{ij} = \left(\frac{C_3 - 2}{C_2 - \frac{4}{3}}\right)\frac{(\tau_{ij} - \frac{2}{3}K\delta_{ij})}{2K}, \tag{36}$$

$$\overline{S}^{*}_{ij} = \tfrac{1}{2}g\frac{K}{\varepsilon}(2 - C_3)\overline{S}_{ij}, \tag{37}$$

$$\overline{W}^{*}_{ij} = \tfrac{1}{2}g\frac{K}{\varepsilon}(2 - C_4)\overline{W}_{ij}, \tag{38}$$

and thus $\overline{\boldsymbol{S}}^{*}$ and $\overline{\boldsymbol{W}}^{*}$ are directly proportional to $\overline{\boldsymbol{S}}$ and $\overline{\boldsymbol{W}}$ so it is only necessary to consider the latter terms. The solution for the coefficients is given by (see Gatski & Speziale 1993)

$$\left.\begin{array}{ll}
G^{(1)} = -\tfrac{1}{2}(6 - 3\eta_1 - 21\eta_2 - 2\eta_3 + 30\eta_4)/D, & G^{(6)} = -9/D, \\
G^{(2)} = -(3 + 3\eta_1 - 6\eta_2 + 2\eta_3 + 6\eta_4)/D, & G^{(7)} = 9/D, \\
G^{(3)} = (6 - 3\eta_1 - 12\eta_2 - 2\eta_3 - 6\eta_4)/D, & G^{(8)} = 9/D, \\
G^{(4)} = -3(3\eta_1 + 2\eta_3 + 6\eta_4)/D, & G^{(9)} = 18/D, \\
G^{(5)} = -9/D, & G^{(10)} = 0,
\end{array}\right\} \tag{39}$$

where the denominator $D$ is

$$\begin{aligned} D = 3 - \tfrac{7}{2}\eta_1 + \eta_1^2 - \tfrac{15}{2}\eta_2 - 8\eta_1\eta_2 + 3\eta_2^2 - \eta_3 + \tfrac{2}{3}\eta_1\eta_3 \\ -2\eta_2\eta_3 + 21\eta_4 + 24\eta_5 + 2\eta_1\eta_4 - 6\eta_2\eta_4 \end{aligned} \tag{40}$$

and

$$\eta_1 = \{\overline{\boldsymbol{S}}^{*2}\}, \quad \eta_2 = \{\overline{\boldsymbol{W}}^{*2}\}, \quad \eta_3 = \{\overline{\boldsymbol{S}}^{*3}\}, \quad \eta_4 = \{\overline{\boldsymbol{S}}^{*}\overline{\boldsymbol{W}}^{*2}\}, \quad \eta_5 = \{\overline{\boldsymbol{S}}^{*2}\overline{\boldsymbol{W}}^{*2}\}.$$

The axial mean velocity gives rise to

$$\overline{\boldsymbol{W}}^{2} = \begin{pmatrix} -\frac{1}{4}\left(\mathrm{d}\bar{u}_z/\mathrm{d}r\right)^2 - \alpha^2\Omega^2 & 0 & 0 \\ 0 & -\alpha^2\Omega^2 & -\frac{1}{2}\alpha\Omega\,\mathrm{d}\bar{u}_z/\mathrm{d}r \\ 0 & -\frac{1}{2}\alpha\Omega\,\mathrm{d}\bar{u}_z/\mathrm{d}r & -\frac{1}{4}\left(\mathrm{d}\bar{u}_z/\mathrm{d}r\right)^2 \end{pmatrix}. \tag{41}$$

Hence, this quadratic generator, like the other quadratic terms, does not contribute a non-zero value to $\tau_{r\theta}$, and thus will not lead to a mean swirl velocity. However, such an effect does come in at the cubic level. In the cubic generator in (35) the axial mean velocity gives rise to the matrix:

$$\overline{\boldsymbol{W}}\,\overline{\boldsymbol{S}}^{2} - \overline{\boldsymbol{S}}^{2}\overline{\boldsymbol{W}} = \begin{pmatrix} 0 & \frac{1}{4}\alpha\Omega\left(\mathrm{d}\bar{u}_z/\mathrm{d}r\right)^2 & 0 \\ \frac{1}{4}\alpha\Omega\left(\mathrm{d}\bar{u}_z/\mathrm{d}r\right)^2 & 0 & 0 \\ 0 & 0 & 0 \end{pmatrix}. \tag{42}$$

The resulting non-zero value for $\tau_{r\theta}$ will generate a mean swirl velocity. The same is true of the other cubic generator, since it is

$$\overline{\boldsymbol{W}}^2\overline{\boldsymbol{S}} + \overline{\boldsymbol{S}}\,\overline{\boldsymbol{W}}^2 = \begin{pmatrix} 0 & -\frac{1}{4}\alpha\Omega\left(\frac{\mathrm{d}\bar{u}_z}{\mathrm{d}r}\right)^2 & -\frac{1}{4}\left(\frac{\mathrm{d}\bar{u}_z}{\mathrm{d}r}\right)^3 - \frac{1}{2}\alpha^2\Omega^2\frac{\mathrm{d}\bar{u}_z}{\mathrm{d}r} \\ -\frac{1}{4}\alpha\Omega\left(\frac{\mathrm{d}\bar{u}_z}{\mathrm{d}r}\right)^2 & 0 & 0 \\ -\frac{1}{4}\left(\frac{\mathrm{d}\bar{u}_z}{\mathrm{d}r}\right)^3 - \frac{1}{2}\alpha^2\Omega^2\frac{\mathrm{d}\bar{u}_z}{\mathrm{d}r} & 0 & 0 \end{pmatrix}. \quad (43)$$

On the other hand, it can be shown that the quartic terms – embodied by $\boldsymbol{T}^{(7)} - \boldsymbol{T}^{(9)}$ in (35) – do not give rise to a non-zero shear component (the quintic term represented by $\boldsymbol{T}^{(10)}$ has a coefficient that is zero). *Thus, it can be concluded that a mean swirl velocity arises from a cubic nonlinearity in conventional explicit algebraic stress models.* This is consistent with the results of Wallin & Johansson (1997). In fact, Craft, Launder & Suga (1993) developed a cubic algebraic model to better describe swirling flows. However, their model suffers a certain basic inconsistency which argues against its use in general flows (Speziale 1998*a*).

### 3.3. *Second-order closure models*

Second-order closure models are based on the Reynolds stress transport equation which, in a rotating frame, takes the form

$$\bar{u}_k\frac{\partial\tau_{ij}}{\partial x_k} = -\tau_{ik}\frac{\partial\bar{u}_j}{\partial x_k} - \tau_{jk}\frac{\partial\bar{u}_i}{\partial x_k} + \Pi_{ij} - \varepsilon_{ij} - \frac{\partial C_{ijk}}{\partial x_k} + \nu\nabla^2\tau_{ij} - 2e_{mki}\Omega_m\tau_{jk} - 2e_{mkj}\Omega_m\tau_{ik} \quad (44)$$

for statistically steady flows, where again $\Omega_m$ is the angular velocity of the reference frame relative to an inertial frame and $e_{ijk}$ is the permutation tensor. Here,

$$\Pi_{ij} \equiv \overline{p'\left(\frac{\partial u_i'}{\partial x_j} + \frac{\partial u_j'}{\partial x_i}\right)}, \quad (45)$$

$$\varepsilon_{ij} \equiv 2\nu\overline{\frac{\partial u_i'}{\partial x_k}\frac{\partial u_j'}{\partial x_k}}, \quad (46)$$

$$C_{ijk} \equiv \overline{u_i'u_j'u_k'} + \overline{p'u_i'}\delta_{jk} + \overline{p'u_j'}\delta_{ik}, \quad (47)$$

are, respectively, the pressure–strain correlation, dissipation rate tensor and turbulent diffusion correlation.

In order to achieve closure of the Reynolds stress transport equation (44), models are needed for:

(*a*) the pressure–strain correlation, $\Pi_{ij}$;
(*b*) the dissipation rate tensor, $\varepsilon_{ij}$;
(*c*) the turbulent diffusion correlation, $C_{ijk}$.

Usually, the Kolmogorov assumption of local isotropy is invoked whereby at high Reynolds numbers it is assumed that (Hinze 1975)

$$\varepsilon_{ij} = \tfrac{2}{3}\varepsilon\delta_{ij}, \quad (48)$$

where the turbulent (scalar) dissipation rate $\varepsilon$ is obtained from a modelled transport

equation of the same general form as (17). The pressure–strain correlation $\Pi_{ij}$ is modelled in an algebraic form based on a simplified analysis of the Poisson equation for the pressure (Reynolds 1987). In the Launder *et al.* (1975) model the following linear form is chosen:

$$\begin{aligned}\Pi_{ij} = &-C_1\varepsilon b_{ij} + C_2 K\overline{S}_{ij} + C_3 K\left(b_{ik}\overline{S}_{jk} + b_{jk}\overline{S}_{ik} - \tfrac{2}{3}b_{mn}\overline{S}_{mn}\delta_{ij}\right)\\ &+C_4 K(b_{ik}\overline{W}_{jk} + b_{jk}\overline{W}_{ik})\end{aligned} \tag{49}$$

where

$$\left.\begin{aligned} b_{ij} &= \frac{\tau_{ij} - \frac{2}{3}K\delta_{ij}}{2K},\\ C_1 &= 3.0, \quad C_2 = 0.8, \quad C_3 = 1.75, \quad C_4 = 1.31\end{aligned}\right\} \tag{50}$$

and, here,

$$\overline{W}_{ij} = \frac{1}{2}\left(\frac{\partial \bar{u}_i}{\partial x_j} - \frac{\partial \bar{u}_j}{\partial x_i}\right) + e_{mji}\Omega_m \tag{51}$$

is the absolute mean vorticity tensor which, in this flow, has the following non-zero components:

$$\overline{W}_{\theta r} = \frac{r}{2}\frac{\partial}{\partial r}\left(\frac{\bar{u}_\theta}{r}\right) + \alpha\Omega = -\overline{W}_{r\theta}, \quad \overline{W}_{zr} = \frac{1}{2}\frac{\partial u_z}{\partial r} = -\overline{W}_{rz}.$$

Launder *et al.* in fact proposed two different variants for the linear model: a quasi-isotropic (QI) representation and a much simpler isotropization-of-production (IP) form in which only the leading term of the QI version was retained. Hirai *et al.* (1988) used the QI model to predict the fully developed flow in an axially rotating pipe with apparent success. However, those authors did not include in their computations the wall-damping terms that are required for the Launder *et al.* models to return approximately correct relative stress levels in the local equilibrium region near a solid wall. The need for such terms to correct the Launder *et al.* models in wall-bounded flows is well documented in the literature. In a recent study Malin & Younis (1997) found that the QI model, when properly used in conjunction with wall-damping terms, yields predictions for the axially-rotating pipe flow that are seriously at variance with measurements. In this study, we shall confine consideration to the IP model, which we will use here with the wall-damping terms proposed by Gibson & Launder (1978).

An alternative formulation to the linear one of Launder *et al.* is that of Speziale, Sarkar & Gatski (1991) (SSG) which is based on the quadratic form

$$\begin{aligned}\Pi_{ij} = &-(C_1\varepsilon + C_1^*\mathscr{P})b_{ij} + C_2^*\varepsilon\left(b_{ik}b_{kj} - \tfrac{1}{3}b_{k\ell}b_{k\ell}\delta_{ij}\right) + (C_2 - C_3^* II_b^{1/2})K\overline{S}_{ij}\\ &+C_3 K\left(b_{ik}\overline{S}_{jk} + b_{jk}\overline{S}_{ik} - \tfrac{2}{3}b_{k\ell}\overline{S}_{k\ell}\delta_{ij}\right) + C_4 K(b_{ik}\overline{W}_{jk} + b_{jk}\overline{W}_{ik}),\end{aligned} \tag{52}$$

where

$$\left.\begin{aligned} &C_1 = 3.4, \quad C_1^* = 1.80, \quad C_2^* = 4.2, \quad C_2 = 0.8,\\ &C_3^* = 1.30, \quad C_3 = 1.25, \quad C_4 = 0.40, \quad II_b = b_{ij}b_{ij}.\end{aligned}\right\} \tag{53}$$

Notice that in the SSG model the rapid part of the pressure–strain correlation is *tensorially* linear. By definition, the rapid pressure–strain correlation is linear in the energy spectrum tensor and, hence, linear in the Reynolds stress tensor (Reynolds 1987). One of the advantages of the SSG model is that it can be applied to wall-bounded geometries without wall reflection terms (Abid & Speziale 1993). The coefficients $C_1$ and $C_2$ in the explicit algebraic stress model (26) are the equilibrium values of $C_1 + C_1^*\mathscr{P}/\varepsilon$ and $C_2 - C_3^* II_b^{1/2}$; $C_3$ and $C_4$ are the same as those given in (53). In the last

decade, cubic models in $b_{ij}$ have been proposed (see e.g. Fu, Launder & Tselepidakis 1987 and Ristorcelli, Lumley & Abid 1995). However, in most instances they do not perform any better. This will be discussed in more detail in the next section.

The Daly & Harlow (1970) model is used for the turbulent diffusion terms since it is the simplest such model. This diffusion model takes the form

$$C_{ijk} = -C_s \frac{K}{\varepsilon} \tau_{km} \frac{\partial \tau_{ij}}{\partial x_m}, \tag{54}$$

where the coefficient $C_s \approx 0.22$. Henceforth, we use the notation

$$\mathscr{D}_{ij} = -\frac{\partial C_{ijk}}{\partial x_k}. \tag{55}$$

Since $\bar{\boldsymbol{u}} = \bar{u}_\theta(r)\boldsymbol{e}_\theta + \bar{u}_z(r)\boldsymbol{e}_z$ it follows that $\bar{\boldsymbol{u}} \cdot \nabla = 0$. Furthermore, at high Reynolds numbers, the molecular diffusion terms can be neglected in the Reynolds stress transport equation (44) and the Kolmogorov assumption of local isotropy can be implemented as given in (48). This yields, from (44), the following transport equation for the Reynolds shear stress $\tau_{r\theta}$, that the axial mean velocity $\bar{u}_z(r)$ gives rise to:

$$\Pi_{r\theta} + \mathscr{D}_{r\theta} - 2\Omega(\tau_{rr} - \tau_{\theta\theta}) = 0. \tag{56}$$

The last term in this equation comes from Coriolis effects, and viscous effects have been neglected for simplicity which can be done at high Reynolds numbers. The leading-order term for $\Pi_{r\theta}$ is the return-to-isotropy term – the first term in (49) and (52) – which takes the form

$$\Pi_{r\theta} = -C_1 \varepsilon \frac{\tau_{r\theta}}{2K} \tag{57}$$

and is present in all second-order closure models. Hence,

$$\frac{C_1 \varepsilon}{2K} \tau_{r\theta} = \Pi_{r\theta}^{(R)} + \mathscr{D}_{r\theta} - 2\Omega(\tau_{rr} - \tau_{\theta\theta}), \tag{58}$$

where $\Pi_{ij}^{(R)}$ is predominantly the rapid part of the pressure–strain correlation which also contains the nonlinear part of the slow pressure–strain correlation (Reynolds 1987). Now, $\tau_{rr}$ and $\tau_{\theta\theta}$ are two of the principal components of the turbulent kinetic energy

$$K = \tfrac{1}{2}(\tau_{rr} + \tau_{\theta\theta} + \tau_{zz}), \tag{59}$$

which is non-zero in any pipe flow. Therefore, $\tau_{rr}$ and $\tau_{\theta\theta}$ are non-zero. Furthermore, they are not equal since pipe flow is known to be anisotropic (all of the components of the turbulent kinetic energy in (59) are unequal except near the centreline of the pipe (Hinze 1975)). So from (58) a non–zero value of $\tau_{r\theta}$ will be predicted yielding a mean swirl velocity $\bar{u}_\theta$ that is rotationally dependent. *Thus, a non-zero mean swirl velocity will be predicted in axially rotating pipe flow by virtually all existing second-order closures by the presence of Coriolis terms.* The simplified Launder *et al.* model (the IP model) yields $\tau_{rr} = \tau_{\theta\theta}$ outside the near-wall region of the pipe so that the mean swirl velocity arises exclusively from wall reflection terms. Since from (44) it follows that

$$\frac{C_1 \varepsilon}{2K} \tau_{rz} = \Pi_{rz}^{(R)} + \mathscr{D}_{rz} + 2\Omega\tau_{\theta z}, \tag{60}$$

it is clear that $\tau_{rz}$ will depend on $\Omega$ since $\tau_{\theta z}$ is non-zero, as we will see later. *Therefore, all second-order closure models predict the rotationally dependent axial mean velocity which is observed experimentally.* While virtually all second-order closures can predict the two main physical features of turbulent flow in an axially rotating pipe, the quality

of the predictions can vary – particularly depending on what pressure–strain model is chosen. In the next section, we show that quadratic pressure–strain models perform the best overall in comparison with experimental data.

## 4. Illustrative calculations

Calculations will be presented relative to both the rotating frame of the pipe and the inertial frame since the latter was used in previous studies (the former, however, greatly simplifies the analysis). Since high Reynolds number flows will be considered, the solutions will be matched to the law of the wall in order to avoid the ambiguities of near-wall modelling. Support for the use in this flow of the conventional log law (suitably extended by reference to the resultant relative velocity and wall shear stress vectors) is provided by the measurements of Kitoh (1991) obtained in a swirling flow in a straight pipe at high Reynolds number. Here, we deduce the resultant wall shear stress from the extended log law and obtain its axial and tangential components – to provide boundary conditions for the velocity components in the same directions – by direct resolution (Gibson & Younis 1986). The mean swirl velocity in the inertial frame is given by

$$\overline{U}_\theta = \bar{u}_\theta + \Omega r, \tag{61}$$

where $\bar{u}_\theta$ is the mean swirl velocity relative to the rotating frame. Thus, when there is the absence of a mean swirl velocity relative to the rotating frame, its profile is linear relative to the inertial frame. The axial mean velocity is the same in both reference frames (i.e. $\overline{U}_z = \bar{u}_z$) since $\bar{u}_z = \bar{u}_z(r)$ and $\boldsymbol{\Omega} = \Omega \boldsymbol{e}_z$.

In figure 2, the predictions of various models for the axial mean velocity and Reynolds shear stress in a stationary circular pipe at a high Reynolds number are shown as a benchmark and compared with the measurements of Imao *et al.* (1996) for a Reynolds number (based on bulk axial mean velocity and pipe radius) of 10 000. (The variable-coefficient SSG model is a non-equilibrium version of this model that has recently been developed; it was ultimately abandoned since it does not appear to make much of a difference in pipe flow). It is clear that all of the models predict the characteristic (flat) turbulent mean velocity profile reasonably well which becomes more pronounced at higher Reynolds numbers. In figure 3, the predictions of several two-equation models for the axial mean velocity in an axially rotating pipe are displayed for a non-dimensional rotation rate of $N = 0.5$ and compared with the experimental data of Imao *et al.* (1996) as well as with the predictions of several second-order closures. Here,

$$N = \frac{\Omega R}{U_0}, \tag{62}$$

where $U_0$ is the bulk axial mean velocity. It is clear from these calculations that, consistent with the results derived in this paper, the $K$–$\varepsilon$ model does not respond to the rotation, incorrectly yielding a mean velocity that is independent of the rotation rate of the pipe (the nonlinear $K$–$\varepsilon$ model yields similar results which are not shown for simplicity). On the other hand, the two-dimensional explicit algebraic stress model based on the SSG model (Gatski & Speziale 1993) responds to the rotation and predicts a reasonably good axial mean velocity in agreement with experiments as shown in figure 3. However, all of these two-equation models predict that the mean swirl velocity $\bar{u}_\theta$ is zero relative to the rotating pipe.

Although the two-dimensional explicit algebraic stress model does not predict the presence of a mean swirl velocity relative to the rotating pipe, it is not that serious from

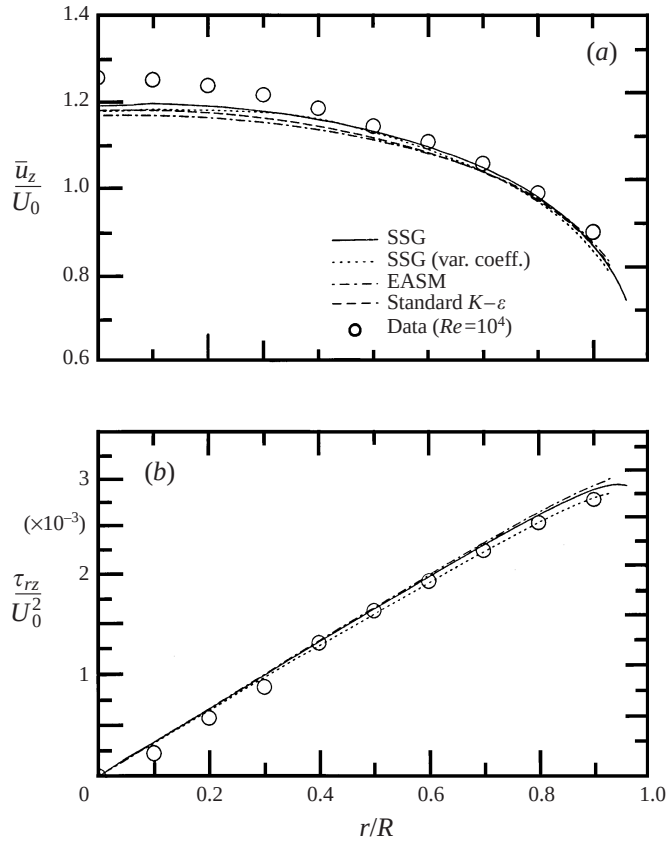


FIGURE 2. Turbulent flow in a stationary circular pipe: comparison of the predictions of various models with experimental data (EASM denotes the explicit algebraic stress model). (*a*) Axial mean velocity and (*b*) Reynolds shear stress. Data of Imao *et al.* (1996).

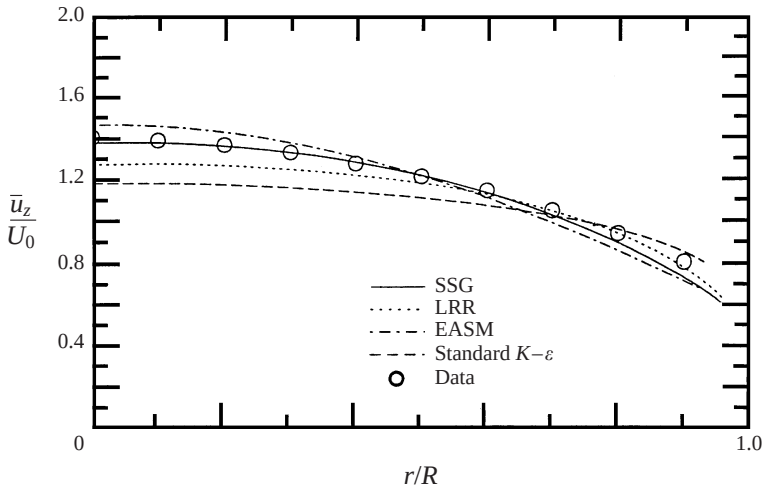


FIGURE 3. Predictions of various two-equation models and second-order closures (LRR is the Launder *et al.* 1975 model) for the axial mean velocity in axially rotating pipe flow. Comparisons are made with the experimental data of Imao *et al.* (1996).

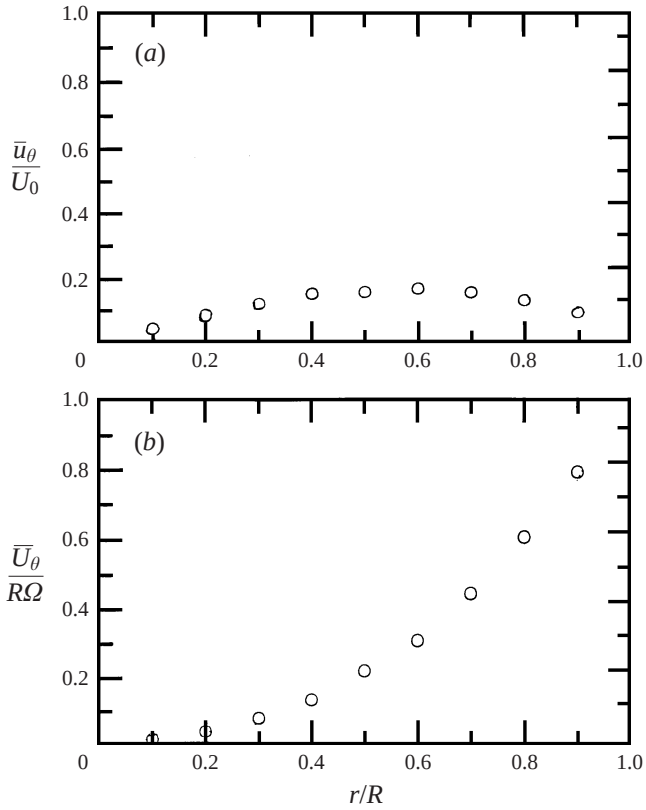


FIGURE 4. Experimental data of Imao *et al.* (1996) for the mean swirl velocity in an axially rotating pipe. (*a*) The mean swirl velocity relative to the rotating pipe normalized by the bulk axial mean velocity and (*b*) the mean swirl velocity relative to the inertial frame normalized by the angular velocity of the pipe in the traditional way.

an engineering standpoint. This mean swirl velocity only constitutes approximately a 15% effect, relative to the axial mean velocity, as shown in figure 4(*a*), when the measurements are taken relative to the rotating pipe and normalized by the bulk axial mean velocity. It appears to be deceptively large when measurements are taken relative to the inertial frame – and normalized in the traditional way with respect to $\Omega R$ – because of the angular velocity of the pipe (see figure 4*b*). Since the two-dimensional explicit algebraic stress model does a good job in predicting the crucial axial mean velocity (there is only approximately a 7–8% error), it is adequate from an engineering standpoint yielding results that are overall only in error of the order of 10%.

In figure 5, it is shown that with a three-dimensional explicit algebraic stress model it is possible to predict the presence of a mean swirl velocity along with a rotationally dependent axial mean velocity. For this purpose, calculations are taken from Wallin & Johansson (1997) where comparisons were made with the experimental data of Imao *et al.* (1996). However, the three-dimensional model used by Wallin & Johansson (1997) only has one of the two cubic generators discussed earlier in § 3.3. This is probably why the specific quantitative agreement is not particularly close (it is, however, fairly good from a qualitative standpoint). We will not present calculations for the full three-dimensional explicit algebraic stress model (Gatski & Speziale 1993) because it is extremely complicated and is in need of regularization which is not

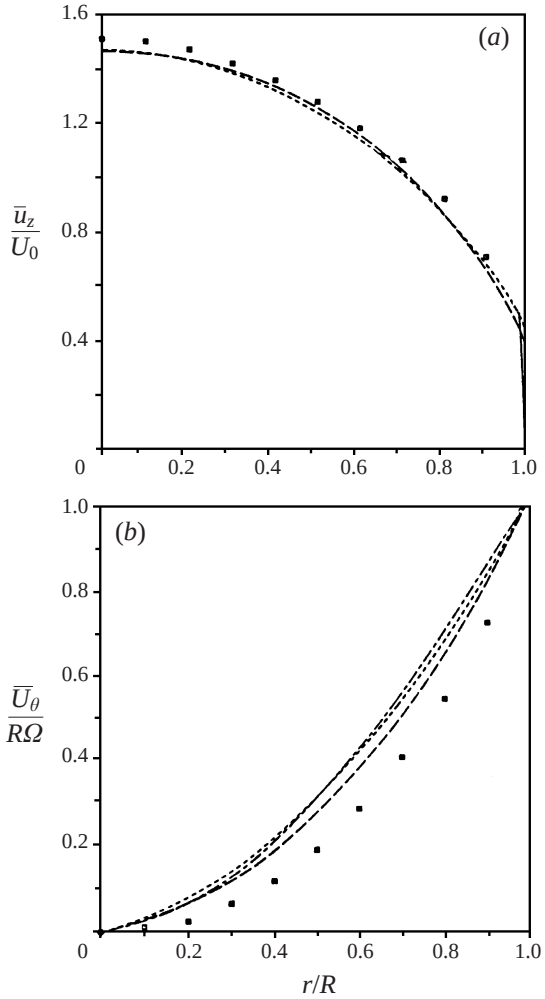


FIGURE 5. Predictions of the cubic algebraic models of Wallin & Johansson (1997) for the mean velocity in an axially rotating pipe compared with the experimental data (●) of Imao *et al.* (1996). (*a*) Axial mean velocity and (*b*) mean swirl velocity relative to the inertial frame. Taken from Wallin & Johansson (1997).

as straightforward as in the two-dimensional case. As mentioned earlier, Craft *et al.* (1993) developed a cubic algebraic model in order to better describe swirling flows.

The results obtained for the axial mean velocity and mean swirl velocity – relative to the rotating pipe – obtained from second-order closures are displayed in figure 6 side by side for the axially rotating pipe ($N = 0.5$). The mean swirl velocity given in the conventional way relative to the inertial frame is shown in figure 7. Again comparisons are made with the experimental data of Imao *et al.* (1996). In figures 8 and 9, the associated Reynolds stresses are provided in detail. Both the Launder *et al.* (1975) model and the SSG model of Speziale *et al.* (1991) are displayed along with the results of the standard $K$–$\varepsilon$ model. It is clear from the results for the mean velocity that the Launder *et al.* model is able to predict both mean effects reasonably well in an axially rotating pipe while the SSG model yields results that are even better. This is generally consistent with our earlier analysis in § 3.3. It should be remembered that second-order closures are equivalent to an algebraic model with a quartic nonlinearity

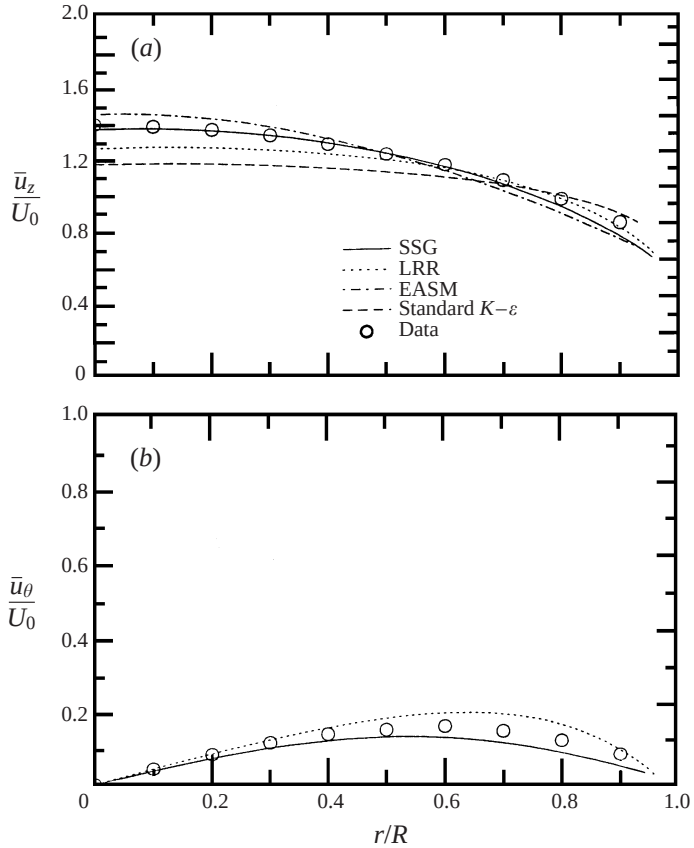


FIGURE 6. Predictions of various second-order closure models for the axial mean velocity and mean swirl velocity relative to the rotating pipe in axially rotating pipe flow. Comparisons are made with the experimental data of Imao *et al.* (1996). (*a*) Axial mean velocity and (*b*) mean swirl velocity relative to the rotating frame.

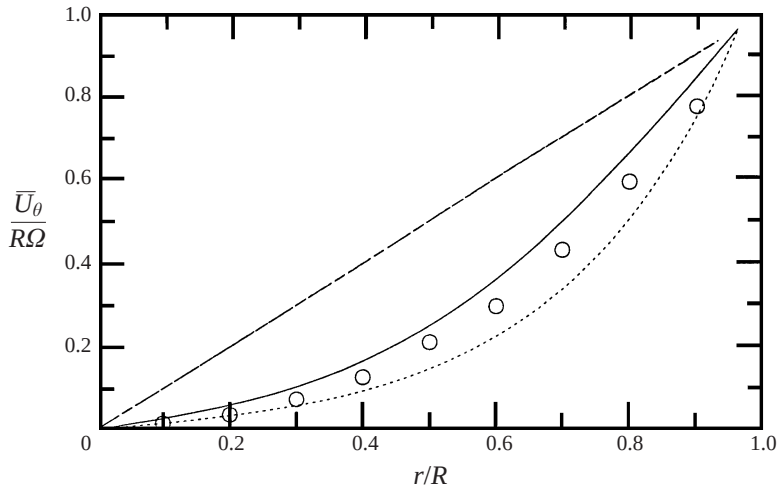


FIGURE 7. Mean swirl velocity relative to the inertial frame predicted by various closure models compared to the experimental data of Imao *et al.* (1996) (○). ——, SSG model; - - -, Launder *et al.* model and – – –, Standard $K$–$\varepsilon$ model.

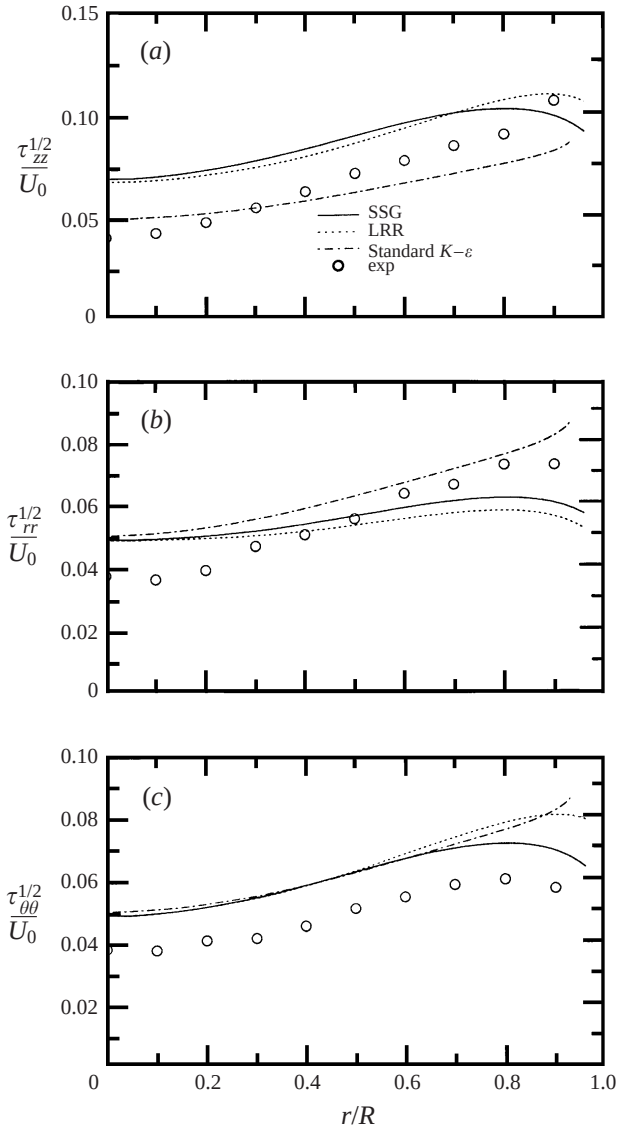


FIGURE 8. Normal Reynolds stresses in the axially rotating pipe. Comparison of the predictions of various second-order closure models and the $K$–$\varepsilon$ model with the experimental data of Imao *et al.* (1996). (*a*) $\tau_{zz}$, (*b*) $\tau_{rr}$, and (*c*) $\tau_{\theta\theta}$.

when the algebraic stress model approximation is made in three dimensions (Gatski & Speziale 1993). This explains why both three-dimensional explicit algebraic stress models and second-order closure models do well. The experimental data for the Reynolds stresses – except for the crucial Reynolds shear stress $\tau_{rz}$ that drives the flow – is probably not that accurate.

These calculations were repeated for the more rapid rotation case of $N = 0.71$. Both the Launder *et al.* model and the SSG model were considered and comparisons were made with the large-eddy simulations of Eggels *et al.* (1994) (comparisons were not made with the direct simulations because of the large disparity in the Reynolds numbers: the Reynolds number of the large-eddy simulations was 59 500). In large-

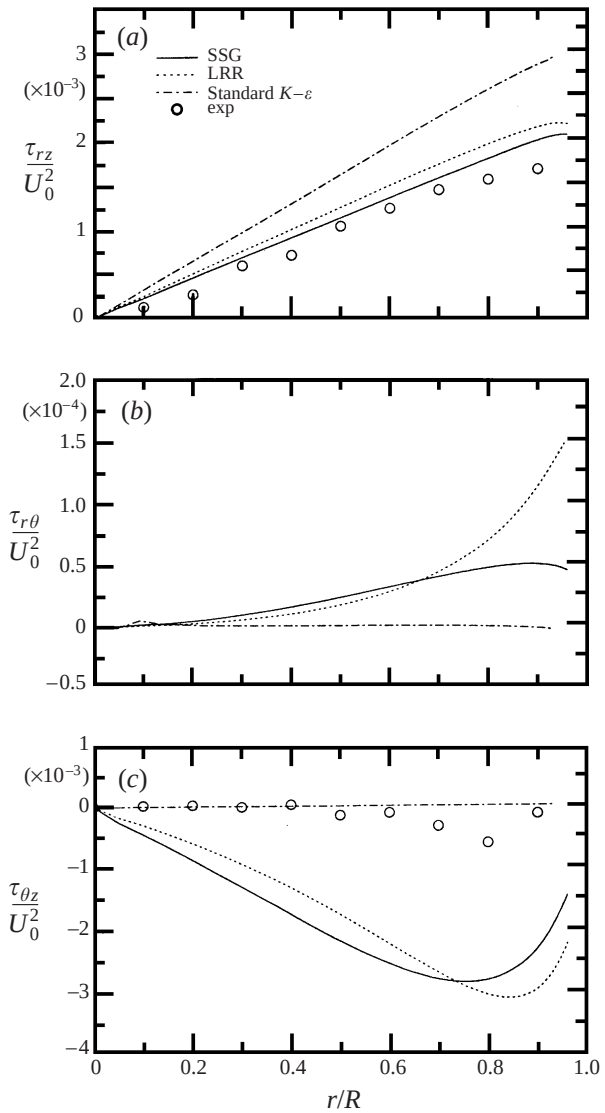


FIGURE 9. Reynolds shear stresses in the axially rotating pipe. Comparison of the predictions of various second-order closure models and the $K$–$\varepsilon$ model with the experimental data of Imao *et al.* (1996). (*a*) $\tau_{rz}$, (*b*) $\tau_{r\theta}$, and (*c*) $\tau_{\theta z}$.

eddy simulations, the full Navier–Stokes equations (1)–(3) are solved numerically with a subgrid-scale stress model. In figure 10*a*, *b* the axial mean velocity and mean swirl velocity relative to the inertial frame are displayed. The Reynolds stresses are not compared in detail due to the problem of defiltering that leads to uncertainties. It appears, however, from the mean velocities that there is no question that second-order closure models provide a good description of this flow (the results of the SSG model are excellent). Furthermore, it is clear from these results that quadratic pressure–strain models – as embodied by the SSG model – perform the best overall consistent with the recent calculations of Pettersson *et al.* (1998).

It should be noted that the profile for $\tau_{r\theta}$ is such that the values for the Reynolds shear stress are zero except close to the wall. From (13) it is clear that in the inviscid

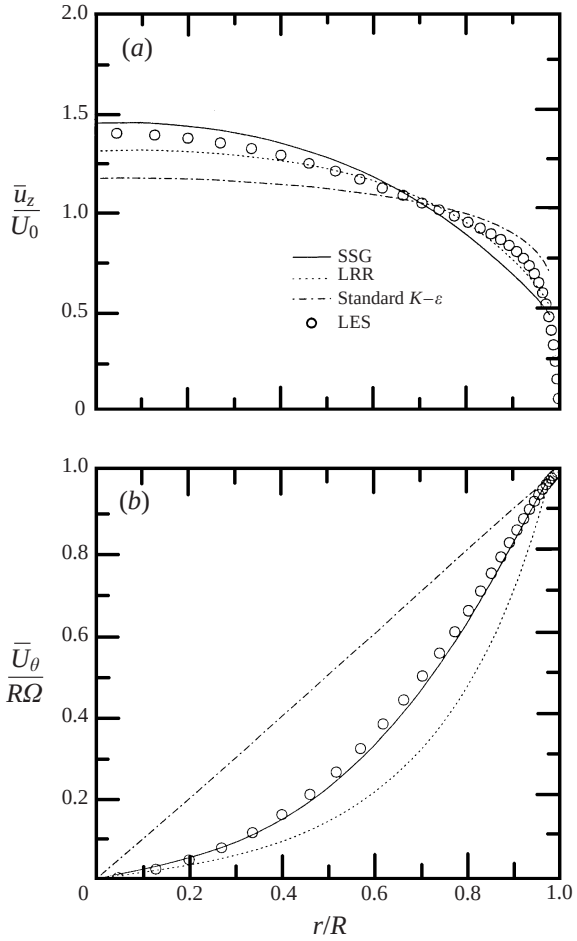


FIGURE 10. Comparison of the predictions of various second-order closure models and the $K$–$\varepsilon$ model for the mean velocity in the axially rotating pipe with the large-eddy simulations of Eggels *et al.* (1994). (*a*) Axial mean velocity and (*b*) the mean swirl velocity relative to the inertial frame.

limit – which is a valid approximation for the case of high Reynolds number flows except for those close to a wall – we have

$$\frac{\mathrm{d}\tau_{r\theta}}{\mathrm{d}r} + \frac{2}{r}\tau_{r\theta} = 0, \tag{63}$$

which has the solution

$$\tau_{r\theta} = \frac{\text{constant}}{r^2}. \tag{64}$$

Regularity of the solution at the centre of the pipe requires that the constant be zero and, thus,

$$\tau_{r\theta} = 0, \tag{65}$$

so that $\tau_{r\theta}$ can only be non-zero in the near-wall region (Yakhot, Private Communication). This is a somewhat surprising result that will be demonstrated by calculations. *Since $\tau_{r\theta}$ is the generator for a mean swirl velocity, we can conclude that a non-zero mean swirl velocity arises largely from near-wall effects in a high-Reynolds-number axially rotating pipe flow*. This is illustrated in figure 11 where the Reynolds number

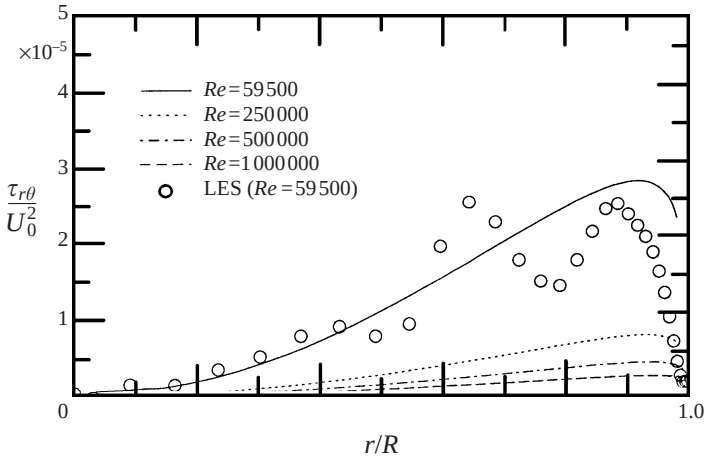


FIGURE 11. Predictions of the SSG model for the Reynolds shear stress $\tau_{r\theta}$ in the axially rotating pipe. The Reynolds number is successively raised starting from the value of the large-eddy simulations (LES) of Eggels *et al.* (1994).

was successively raised starting from the value of the large-eddy simulations. Clearly, from these results, $\tau_{r\theta}$ goes to zero as $Re \to \infty$ consistent with these theoretical results. Furthermore, these results demonstrate the difficulty of large-eddy simulations in accurately determinating the Reynolds stresses (notice in figure 11 the waves in the profile of the Reynolds shear stress obtained from the large-eddy simulations).

Note that formally the solution of the modified Helmholtz equation (13) for the mean swirl velocity can be written as

$$\bar{u}_\theta = \int_R G(\boldsymbol{x}, \boldsymbol{x}') \frac{1}{\nu r'^2} \frac{\mathrm{d}}{\mathrm{d}r'} (r'^2 \tau'_{r\theta}) \, \mathrm{d}^3 x' \tag{66}$$

plus surface terms (where $R$ is the region of the pipe and $G(\boldsymbol{x}, \boldsymbol{x}')$ is the Green's function). Here, the Green's function (Morse & Feshbach 1953) is such that

$$G(\boldsymbol{x}, \boldsymbol{x}') \sim \frac{1}{|\boldsymbol{x} - \boldsymbol{x}'|}, \tag{67}$$

so that even though $\tau_{r\theta}$ is confined to the near-wall region $\bar{u}_\theta$ will be non-zero throughout the pipe consistent with experimental observations (see the experimental data illustrated in figure 4). Thus, in principle, a non-zero mean swirl velocity can be predicted by the $K$–$\varepsilon$ model if a more sophisticated near-wall treatment is implemented, namely one that predicts a non-zero $\tau_{r\theta}$ in the near-wall region. While it may not be desirable to do this, it is, in principle, possible. Of course, any standard near-wall treatment in conventional two-equation models will yield $\tau_{r\theta}$ – and, hence, $\bar{u}_\theta$ – equal to zero as discussed earlier.

According to the Taylor–Proudman theorem, a flow will two-dimensionalize when subjected to a rapid rotation (Tritton 1977). This will also tend to cause the flow to laminarize, which explains why the axial velocity profiles become more laminar-like when there is a discernible rotation. This effect can be observed in figure 3 and figure 10. The development of a turbulence model that is fully consistent with the Taylor–Proudman theorem is a very challenging undertaking that has not yet been fully achieved (Speziale 1998*b*). It also requires a modification in the dissipation rate equation to account for rotational effects (Speziale & Gatski 1997). Rotations disturb the energy cascade causing the dissipation to be reduced.

Finally, some comments are warranted concerning the possible development of a symmetry-breaking bifurcation (i.e. a bifurcation where there can be an azimuthal dependence) in the axially rotating pipe. A non-zero mean swirl velocity could develop in simple turbulence models through the breakdown of azimuthal symmetry in the Reynolds-averaged equations – i.e. through a symmetry-breaking bifurcation. This would cause there to be a non-zero $\partial\overline{P}/\partial\theta$ that could then generate a non-zero mean swirl velocity in (7). The possible development of a symmetry-breaking bifurcation was tested for computationally. No such bifurcation was found. Whenever a non-zero mean swirl velocity was added, without assumed azimuthal symmetry, it decayed to zero. This was done in the standard two-equation models (i.e. the $K$–$\varepsilon$ model) as well as in the two-dimensional explicit algebraic stress model. Thus, it does not appear that a mean swirl velocity can be generated in these models by such a bifurcation.

## 5. Conclusion

Both the analysis and modelling of turbulent flow in an axially rotating pipe have been considered in depth. Four major conclusions have been arrived at:

(i) The two major effects in this flow – a rotationally dependent axial mean velocity and the presence of mean swirl velocity relative to the rotating pipe – cannot be predicted by traditional two-equation models such as the standard $K$–$\varepsilon$ model with conventional near-wall treatments.

(ii) Two-dimensional explicit algebraic stress models are able to predict the first effect – namely a rotationally dependent axial mean velocity – quite well from a quantitative standpoint. However, they are unable to predict the presence of a non-zero mean swirl velocity – approximately a 15% effect – when conventional near-wall treatments, such as those used in the $K$–$\varepsilon$ model, are implemented. This effect, however, can be predicted by three-dimensional explicit algebraic stress models where it arises from a frame-dependent cubic nonlinearity. There is a problem, however, in that these models erroneously predict that $\tau_{r\theta}$ is non-zero in the inviscid limit, which is the same as the high Reynolds number limit, whereas $\tau_{r\theta} = 0$ according to (13) when $\nu$ goes to zero (this means that the model will yield incorrect predictions at high Reynolds numbers when there are no walls).

(iii) Second-order closure models provide a good description of this flow, in that the two principal effects discussed above can be described by virtually any second-order closure, since they arise from Coriolis effects which are automatically present in these models. Quadratic pressure–strain models – as embodied by the SSG model – performed the best overall when detailed comparisons were made with experiments. The Launder *et al.* model – with its linear pressure–strain – yields a reasonably good description of this flow, but does not perform quite as well.

(iv) The presence of a mean swirl velocity is generated by a non-zero Reynolds shear stress $\tau_{r\theta}$ which, at high Reynolds numbers, is confined to the near-wall region. Thus, even though its effects are felt throughout the pipe, the generation of a non-zero mean swirl velocity is largely a near-wall effect at high Reynolds numbers. Hence, it is possible to predict this effect at high Reynolds numbers with traditional two-equation models if a more sophisticated near-wall treatment that predicts a non-zero $\tau_{r\theta}$, consistent with experimental observations, is implemented. However, it may be undesirable to do so, particularly to be able to properly describe low Reynolds number turbulence.

There is no question that three-dimensional frame-dependent models are needed to adequately describe turbulent flow in an axially rotating pipe. These can be either three-dimensional algebraic models with a cubic nonlinearity or full second-

order closures, although there are some problems with the former. Most existing second-order closure models have pressure–strain that have been developed for two-dimensional mean turbulent flows that are close to equilibrium. This is decidedly the case in the SSG model and is implicit in the Launder *et al.* model. However, since second-order closures contain production and Coriolis terms – which are exact terms that account for three-dimensional effects – they can be applied to this three-dimensional problem. Furthermore, it should be noted that if a more sophisticated near-wall modelling approach is used to predict this flow with simpler two-equation models it must account for three-dimensional frame-dependent effects. This transcends the issue of non-alignment of stress and strain which requires the use of anisotropic eddy viscosity models, at the minimum, to obtain a good description of this flow. Three-dimensionality as well as anisotropy is needed. This is lacking in most simple turbulence models. The problem of turbulent flow in an axially rotating pipe is one of the simplest three-dimensional turbulent flows that can be constructed and yet, as shown in this paper, is one that poses a severe test for current turbulence closures.

This work has arisen from collaboration between the authors while all were in residence at ICASE–NASA Langley Research Centre. We are grateful to Professor M. Y. Hussaini who, as the then Director of ICASE, made this work possible. The first author (C.G.S.) was supported by the Office of Naval Research under Grant N00014-94-1-0088 (*ARI on Nonequilibrium Turbulence*, Dr L. P. Purtell, Program Officer). Our appreciation goes to Dr V. Y. Yakhot (Boston University) for several helpful comments and to Professor S. Imao (Gifu University) for providing us with tabulated experimental data.

## Appendix

We briefly discuss here the laminar non-Newtonian version of this problem. For laminar non-Newtonian flow, the equations of motion for the axially rotating pipe – under fully developed conditions with azimuthal symmetry – take the form

$$-\frac{u_\theta^2}{r} = -\frac{\partial P}{\partial r} - \frac{\mathrm{d}t_{rr}^N}{\mathrm{d}r} - \frac{1}{r}(t_{rr}^N - t_{\theta\theta}^N) + 2\Omega u_\theta, \tag{A 1}$$

$$\nu\left(\nabla^2 u_\theta - \frac{u_\theta}{r^2}\right) - \frac{\mathrm{d}t_{r\theta}^N}{\mathrm{d}r} - \frac{2}{r}t_{r\theta}^N = 0, \tag{A 2}$$

$$-\frac{\partial P}{\partial z} + \nu\nabla^2 u_z - \frac{\mathrm{d}t_{rz}^N}{\mathrm{d}r} - \frac{1}{r}t_{rz}^N = 0, \tag{A 3}$$

where $t_{rr}^N, t_{\theta\theta}^N, t_{r\theta}^N$ and $t_{rz}^N$ are components of the kinematic form of the non-Newtonian viscous stress tensor $t_{ij}^N$. Here, the total stress $t_{ij}$ is given by

$$t_{ij} = -p\delta_{ij} + \mu\left(\frac{\partial u_i}{\partial x_j} + \frac{\partial u_j}{\partial x_i}\right) - \rho t_{ij}^N, \tag{A 4}$$

where $\mu$ is the dynamic viscosity and $p$ is the dynamic pressure ($\nu \equiv \mu/\rho$ and $P \equiv p/\rho$ given that $\rho$ is the mass density which is constant). Equations (A 1)–(A 3) are identical in form to (12)–(14). That is why analogies are often made between the laminar flow of a non-Newtonian fluid and the mean turbulent flow of a Newtonian fluid (and, hence, between the velocity $\boldsymbol{u}$ and the mean velocity $\overline{\boldsymbol{u}}$ as well as between the non-Newtonian viscous stress tensor $t_{ij}^N$ and the Reynolds stress tensor $\tau_{ij}$; see Rivlin 1957;

Hinze 1975). The slow steady flow of dilute non-Newtonian fluids can be described by the Rivlin–Ericksen fluid model for which

$$t_{ij}^N = \alpha_{(M+1)} A_{ij}^{(M+1)} + \alpha_{(M)} A_{ij}^{(M)} + \cdots + \alpha_{(2)} A_{ij}^{(2)}, \tag{A 5}$$

where $\alpha_{(M)}$ are coefficients and $A_{ij}^{(M)}$ is the $M$th Rivlin–Ericksen tensor that is obtained from a recursion relation which, for steady flows, is given by (Eringen 1967)

$$A_{ij}^{(M+1)} = \boldsymbol{u} \cdot \nabla A_{ij}^{(M)} + A_{ik}^{(M)} \frac{\partial u_k}{\partial x_j} + A_{jk}^{(M)} \frac{\partial u_k}{\partial x_i}, \tag{A 6}$$

with

$$A_{ij}^{(1)} = 2S_{ij} \tag{A 7}$$

given that

$$S_{ij} = \frac{1}{2}\left(\frac{\partial u_i}{\partial x_j} + \frac{\partial u_j}{\partial x_i}\right) \tag{A 8}$$

is the rate-of-strain tensor. They are obtained for general simple fluids by an expansion (Truesdell & Noll 1965). The Rivlin–Ericksen fluids are known to have unidirectional flow solutions in a stationary straight pipe where $\boldsymbol{u} = u_z(r)\boldsymbol{e}_z$ so that $t_{r\theta}^N$ is zero (Truesdell & Noll 1965; Schowalter 1978). They are frame-indifferent, so solutions for $t_{ij}^N$ are independent of $\Omega$ (Truesdell & Noll 1965). Thus, no swirl velocity will be present in an axially rotating pipe and the axial mean velocity will be rotationally independent.

## REFERENCES


Abid, R. & Speziale, C. G. 1993 Predicting equilibrium states with Reynolds stress closures in channel flow and homogeneous shear flow. *Phys. Fluids* A **5**, 1776–1782.

Batchelor, G. K. 1967 *An Introduction to Fluid Dynamics*. Cambridge University Press.

Benton, G. S. 1956 The effect of the earth's rotation on laminar flow in pipes. *Trans. ASME: J. Appl. Mech.* **23**, 123–127.

Berger, S. A., Talbot, L. & Yao, L.-S. 1983 Flow in curved pipes. *Ann. Rev. Fluid Mech.* **15**, 461–512.

Craft, T. J., Launder, B. E. & Suga, K. 1993 Development and application of a cubic eddy viscosity model of turbulence. In *Proc. Intl Symp. on Refined Flow Modelling and Turbulence Measurements*, *Paris*, pp. 125–132.

Daly, B. J. & Harlow, F. H. 1970 Transport equations in turbulence. *Phys. Fluids* **13**, 2634–2649.

Dennis, S. C. R. & Ng, M. 1982 Dual solutions for steady laminar flow through a curved tube. *Q. J. Mech. Appl. Maths* **35**, 305–324.

Eggels, J. G. M., Boersma, B. J. & Nieuwstadt, F. T. M. 1994 Direct and large-eddy simulation of turbulent flow in an axially rotating pipe. *Preprint*.

Eggels, J. G. M. & Nieuwstadt, F. T. M. 1993 Large-eddy simulations of turbulent flow in an axially rotating pipe. In *Proc. 9th Symp. on Turbulent Shear Flows, Kyoto, Japan*, pp. 310–313.

Eringen, A. C. 1967 *Mechanics of Continua*. Wiley.

Fu, S., Launder, B. E. & Tselepidakis, D. P. 1987 Accommodating the effects of high strain rates in modelling the pressure–strain correlation. *UMIST Tech. Rep.* TFD/87/5.

Gatski, T. B. & Speziale, C. G. 1993 On explicit algebraic stress models for complex turbulent flows. *J. Fluid Mech.* **254**, 59–78.

Gibson, M. M. & Launder, B. E. 1978 Ground effects on pressure fluctuations in the atmospheric boundary layer. *J. Fluid Mech.* **86**, 491–511.

Gibson, M. M. & Younis, B. A. 1986 Calculation of boundary layers with sudden transverse strain. *Trans. ASME: J. Fluids Engng* **108**, 470–475.

Hinze, J. O. 1975 *Turbulence*, 2nd edn. McGraw-Hill.

Hirai, S., Takagi, T. & Matsumoto, M. 1988 Prediction of the laminarization phenomena in an axially rotating pipe. *Trans. ASME: J. Fluids Engng* **110**, 424–430.

Howard, J. H., Patankar, V. S. & Bordynuik, R. M. 1980 Flow prediction in rotating ducts using Coriolis modified turbulence models. *Trans. ASME: J. Fluids Engng* **102**, 456–461.

Imao, S., Itoh, M. & Harada, T. 1996 Turbulent characteristics of the flow in an axially rotating pipe. *Intl J. Heat Fluid Flow* **17**, 444–451.

Kikuyama, K., Murakami, M. & Nishibori, K. 1983*a* Development of three-dimensional turbulent boundary layer in an axially rotating pipe. *Trans. ASME: J. Fluids Engng* **110**, 154–160.

Kikuyama, K., Murakami, M., Nishibori, K. & Maeda, K. 1983*b* Flow in an axially rotating pipe (a calculation of the separated region). *Bull. JSME* **26**, 506–513.

Kitoh, O. 1991 Experimental study of turbulent swirling flow in a straight pipe. *J. Fluid Mech.* **225**, 445–479.

Laufer, J. 1954 The structure of turbulence in fully-developed pipe flow. *NACA Rep.* 1174.

Launder, B. E., Reece, G. J. & Rodi, W. 1975 Progress in the development of a Reynolds stress turbulence closure. *J. Fluid Mech.* **68**, 537–566.

Majumder, A. K., Pratap, V. S. & Spalding, D. B. 1977 Numerical computation of flow in rotating ducts. *Trans. ASME: J. Fluids Engng* **99**, 148–153.

Malin, M. R. & Younis, B. A. 1997 The prediction of turbulent transport in an axially rotating pipe. *Intl Commum. Heat Mass Transfer* **24**, 89–98.

Morse, P. M. & Feshbach, H. 1953 *Methods of Theoretical Physics.* McGraw-Hill.

Murakami, M. & Kikuyama, K. 1980 Turbulent flow in axially rotating pipes. *Trans. ASME: J. Fluids Engng* **102**, 97–103.

Orlandi, P. & Fatica, M. 1997 Direct simulations of turbulent flow in a pipe rotating about its axis. *J. Fluid Mech.* **143**, 43–72.

Pettersson, B. A., Andersson, H. I. & Brunvoll, A. S. 1998 Modelling near-wall effects in axially rotating pipe by elliptic relaxation. *AIAA J.* **36**, 1164–1170.

Pope, S. B. 1975 A more general effective viscosity hypothesis. *J. Fluid Mech.* **72**, 331–340.

Prandtl, L. 1925 Über die ausgebildete turbulenz. *Z. Angew. Math. Mech.* **5**, 136–139.

Reich, G. & Beer, H. 1989 Fluid flow and heat transfer in axially rotating pipe I. Effect of rotation on turbulent pipe flow. *Intl J. Heat Mass Transfer* **32**, 551–561.

Reynolds, W. C. 1987 Fundamentals of turbulence for turbulence modelling and simulation. In *Lecture Notes for Von Kármán Institute.* AGARD Lecture Series 86, pp. 1–66, NATO.

Ristorcelli, J. R., Lumley, J. L. & Abid, R. 1995 A rapid-pressure correlation representation consistent with the Taylor–Proudman theorem materially-frame-indifferent in the 2-D limit. *J. Fluid Mech.* **292**, 111–152.

Rivlin, R. S. 1957 The relation between the flow of a non-Newtonian fluid and turbulent Newtonian fluid. *Q. Appl. Maths* **15**, 212–215.

Schowalter, W. R. 1978 *Mechanics of Non-Newtonian Fluids.* Pergamon.

Speziale, C. G. 1987 On nonlinear $K$–$\ell$ and $K$–$\varepsilon$ models of turbulence. *J. Fluid Mech.* **178**, 459–475.

Speziale, C. G. 1998*a* A consistency condition for nonlinear algebraic Reynolds stress models in turbulence. *Intl J. Nonlinear Mech.* **33**, 579–584.

Speziale, C. G. 1998*b* A review of material frame-indifference in mechanics. *Appl. Mech. Rev.* **51**, 489–504.

Speziale C. G. & Gatski, T. B. 1997 Analysis and modelling of anisotropies in the dissipation rate of turbulence. *J. Fluid Mech.* **344**, 155–180.

Speziale, C. G., Sarkar, S. & Gatski, T. B. 1991 Modelling the pressure-strain correlation of turbulence: An invariant dynamical systems approach. *J. Fluid Mech.* **227**, 245–272.

Speziale, C. G. & Xu, X. H. 1996 Towards the development of second-order closure models for non-equilibrium turbulent flows. *Intl J. Heat Fluid Flow* **17**, 238–244.

Tritton, D. J. 1977 *Physical Fluid Dynamics.* Van Nostrand.

Truesdell, C. & Noll, W. 1965 The non-linear field theories of mechanics. *Handbuch der Physik* 111/3. Springer.

Wallin, S. & Johansson, A. V. 1997 A new explicit algebraic Reynolds stress turbulence model for 3D flows. In *Proc. 11th Symp. on Turbulent Shear Flows, Institut National Polytechnique de Grenoble, Université Joseph Fourier, Grenoble, France*, pp. 13.13–13.17.

Wallin, S. & Johansson, A. V. 2000 An explicit algebraic Reynolds stress model for incompressible and compressible turbulent flows. *J. Fluid Mech.* **403**, 89–132.

Younis, B. A., Gatski, T. B. & Speziale, C. G. 1996 Assessment of the SSG pressure–strain model in free turbulent jets with and without swirl. *Trans. ASME: J. Fluids Engng* **116**, 800–809.